Supporting Information for

Synthesis, Characterization, and Reactivity of Ethynyl- and Propynyl-Terminated Si(111) Surfaces

Noah T. Plymale,[†] Youn-Geun Kim,[‡] Manuel P. Soriaga,[‡,⊥] Bruce S. Brunschwig,[‡,§] and Nathan S. Lewis*[,†,‡,§,∥]

[†]*Division of Chemistry and Chemical Engineering,* [‡]*Joint Center for Artificial Photosynthesis*, [§]*Beckman Institute*, and [∥]*Kavli Nanoscience Institute*, *California Institute of Technology, Pasadena, California 91125, United States*

[⊥]*Department of Chemistry, Texas A&M University, College Station, Texas 77843, United States*

*Author to whom correspondence should be addressed, *e-mail: nslewis@caltech.edu*

A. Supporting Experimental Details.

1. Preparation of Atomically Flat H–Si(111) Surfaces. Wafers were cut with a diamond-tipped scribe to the desired size and then rinsed sequentially with water, methanol (≥99.8%, EMD), acetone (≥99.5%, EMD), methanol, and water. Organic contaminants were removed and the surfaces were oxidized by immersing the wafers in a freshly prepared piranha solution (1:3 v/v of 30% H_2O_2(aq) (EMD): 18 M H_2SO_4 (EMD)) at 90–95 °C for 10–15 min. The wafers were rinsed with copious amounts of water and immersed in buffered HF(aq) (semiconductor grade, Transene Co., Inc.) for 18 s followed by another water rinse. Atomically flat H–Si(111) surfaces were prepared by immersing the wafers in an Ar(g)-purged solution of NH_4F(aq).[1-2] Wafers with a miscut angle of 0.5° were etched for 5.5 min, while wafers with a miscut angle of 0.1° were etched for 9.0 min to obtain optimal terrace size. The solution was purged throughout the etching process and the wafers were agitated after each minute of etching to remove bubbles

that formed on the surface. After etching, the wafers were rinsed with water and dried under a stream of Ar(*g*).

2. Preparation of Cl–Si(111) Surfaces. Cl–Si(111) surfaces were prepared inside a N_2(g)-purged glovebox with <10 ppm O_2. A saturated solution of PCl_5 (≥99.998% metal basis, Alfa Aesar) in chlorobenzene (anhydrous, ≥99.8%, Sigma-Aldrich) was preheated with an initiating amount (<1 mg mL^{-1}) of benzoyl peroxide (≥98%, Sigma-Aldrich) for 1–2 min. The H–Si(111) wafers were rinsed with chlorobenzene and then reacted in the PCl_5 solution at 90 ± 2 °C for 45 min.[1, 3] Upon completion of the reaction, the solution was drained and the wafers were rinsed with copious amounts of chlorobenzene, followed by tetrahydrofuran (THF, anhydrous, inhibitor-free, ≥99.9%, Sigma-Aldrich).

3. Preparation of of Br–Si(111) Surfaces. Br–Si(111) surfaces were prepared by reaction under ambient light at 22 °C of H–Si(111) with Br_2(g) in a drying chamber connected to a vacuum line as well as to a reservoir of Br_2(l). Immediately after anisotropic etching, H–Si(111) samples were placed inside the drying chamber, which was then evacuated to <20 mTorr. The sample was sealed under vacuum and the Br_2(l) reservoir was quickly opened and closed to allow a visible amount of Br_2(g) into the evacuated drying chamber. The reaction was allowed to proceed for 10 s, after which the Br_2(g) was removed by vacuum to a pressure of <20 mTorr.[2, 4] The sample was sealed under vacuum and transferred to a N_2(g)-purged glovebox.

B. Supporting Instrumentation Details.

1. Transmission Infrared Spectroscopy. A custom attachment allowed Si samples (1.3 × 3.2 cm) to be mounted such that the incident IR beam was either 74° or 30° with respect to the sample surface normal. At 74° (Brewster's angle for Si), IR modes parallel and perpendicular to the surface are observed, and at 30°, parallel modes remain visible, while perpendicular modes

are greatly diminished in intensity.[5] Reported spectra are averages of 1500 consecutive scans collected at a resolution of 4 cm^{-1}. The baseline was flattened and peaks resulting from water absorption were subtracted in the reported spectra. Background SiO_x and H–Si(111) spectra were recorded separately for each sample prior to subsequent functionalization.

2. X-ray Photoelectron Spectroscopy. Photoelectrons were collected at 90° with respect to the surface plane of the sample, with the lens aperture set to sample a 700 × 300 μm spot. The instrument was operated by Vision Manager software v. 2.2.10 revision 5. Survey and high-resolution scans were collected with analyzer pass energies of 80 eV and 10 eV, respectively. No signals from Cl, Br, Mg, Na, or Li impurities were detected on alkylated samples prepared as described. When HCC–Si(111) surfaces were prepared using DMA as the solvent, however, residual Br and N were often observed by XPS.

Thermal stability in vacuum was studied by collecting XP spectra as a function of annealing temperature. Samples were mounted on a resistive heating stage that consisted of a molybdenum puck heated with a tungsten wire. Stainless-steel clips affixed the sample to the molybdenum stage. The temperature was monitored by a type E thermocouple gauge affixed on the molybdenum stage immediately below the sample. Samples were heated to the desired temperature at a ramp rate of 10 °C min^{-1} and were held at the indicated temperature for 30 min. The samples were allowed to cool to 22–30 °C prior to collection of XPS data.

3. Surface Recombination Velocity Measurements. Electron-hole pairs were formed by a 20 ns, 905 nm laser pulse from an OSRAM diode laser with an ETX-10A-93 driver. For each laser pulse, the decay in reflected microwave intensity was monitored by a PIN diode connected to an oscilloscope. All recorded decay curves were averages of 64 consecutive decays. Between measurements, samples were stored in air-filled centrifuge tubes in the dark.

C. Data Analysis.

1. Fitting and Quantification of XPS Data. High-resolution XP spectra were analyzed using CasaXPS software v. 2.3.16. The peak positions for XP spectra were calibrated using the Si $2p_{3/2}$ peak, which was set to be centered at 99.68 eV.[6] For bulk Si^0 and Si^{1+} doublets, the ratio of the peak area of the Si $2p_{1/2}$:$2p_{3/2}$ was set to 0.51 and the width of the two peaks was set equal.[6] Shirley backgrounds were used for all high-resolution data except when analyzing small amounts of SiO_x in the 102–104 eV range, for which a linear background was applied. C 1s and F 1s high-resolution spectra were fitted using the Voigt function GL(30), which consists of 70% Gaussian and 30% Lorentzian character. Si 2p photoemission signals for bulk Si^0 and Si^{1+} species were fitted using asymmetric Lorentzian line shapes convoluted with a Gaussian of the form LA(*a*, *b*, *n*), where *a* and *b* determine the asymmetry of the line shape and *n* specifies the Gaussian width of the function. LA(1.2, 1.4, 200) was found to fit consistently. Contributions from high-order SiO_x in the range of 102–104 eV were fit to a single peak using the GL(30) function.

The thickness (d_A) of the overlayer species A was estimated by XPS for CH_3–Si(111), HCC–Si(111), and CH_3CC–Si(111) surfaces using the substrate-overlayer model[7-8]

$$\left(\frac{I_A}{I_{Si}}\right)\left(\frac{SF_{Si}}{SF_A}\right)\left(\frac{\rho_{Si}}{\rho_A}\right)=\left(\frac{1-e^{\frac{-d_A}{\lambda_A \sin\theta}}}{e^{\frac{-d_A}{\lambda_{Si}\sin\theta}}}\right) \qquad \text{(S1)}$$

where I_A is the area under the photoemission peak arising from the overlayer species A, I_{Si} is the area under the Si 2p photoemission signal, SF_{Si} is the instrument sensitivity factor for Si 2p (0.328), and SF_A is the instrument sensitivity factor for the overlayer species A, which is 0.278 for C 1s photoelectrons in hydrocarbon overlayers. For the hydrocarbon overlayers, I_A is the total area under the C 1s photoemission signal corresponding to all C atoms in the overlayer, which is

the signal at 284.3 eV for CH_3–Si(111) surfaces, the signal at 284.5 eV for HCC–Si(111) surfaces, and the signals at 284.3 and 285.3 eV for CH_3CC–Si(111) surfaces. For Si–OH, I_A is the sum of the area under the Si 2p photoemission signal at 100.5 eV and 101.1 eV. For SiO_x, I_A is the area under the Si 2p photoemission signal appearing from 102–104 eV. The density of Si (ρ_{Si}) is 2.3 g cm^{-3}, and the density of the overlayer species A (ρ_A) is 3.0 g cm^{-3} for hydrocarbon overlayers.[9] HCC–Si(111) surfaces exhibited a fractional monolayer (ML) coverage of ~0.63 ML, so the assumed density of the overlayer was adjusted to model an overlayer with 63% of the density of a full monolayer (1.9 g cm^{-3}). When estimating the thickness of Si–OH or SiO_x overlayers, the quantity $(SF_{Si}/SF_A)(\rho_{Si}/\rho_A)$ reduces to a normalizing constant of 1.3 to account for the difference in Si 2p photoelectron signal intensity for Si–OH or SiO_x relative to bulk Si.[8] The attenuation length for the overlayer species (λ_A) has been estimated to be 3.6 nm for C 1s photoelectrons moving through hydrocarbon overlayers[10-11] or 3.4 nm for Si 2p photoelectrons moving through Si–OH or SiO_x overlayers.[10-11] The attenuation length for Si 2p photoelectrons (λ_{Si}) moving through hydrocarbon overlayers has been estimated to be 4.0 nm.[10-11] For Si–OH or SiO_x overlayers, the value of $\lambda_A = \lambda_{Si} = 3.4$ nm. The angle between the surface plane and the photoelectron ejection vector (θ) is 90°. The thickness of the overlayer species A was calculated using an iterative process.

The fractional monolayer coverage for the overlayer species A (Φ_A) was estimated by dividing the measured thickness, d_A, by the calculated thickness of 1 ML of overlayer species A, depicted in Scheme S1. The thickness of 1 ML of each hydrocarbon overlayer was estimated by summing the bond lengths for the species containing C, but excluding Si and H. For Si–OH overlayers, the thickness of 1 ML was estimated to be the distance from the bottom of the atop Si atom to the top of the O atom. The thickness of 1 ML of SiO_x was estimated to be 0.35 nm.[8, 12]

Assuming uniform overlayers, the value of Φ_A represents the fraction of surface Si(111) sites that were modified with the overlayer species of interest.

Scheme S1.

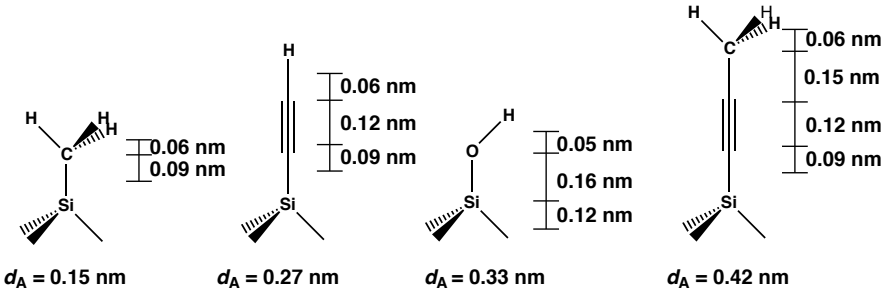

The fractional monolayer coverage for 4-fluorobenzyl-modified HCC–Si(111) and SiO_x surfaces was estimated using a three-layer model[13-14]

$$\left(\frac{I_A}{I_{Si}}\right)\left(\frac{SF_{Si}}{SF_A}\right)\left(\frac{\rho_{Si}}{\rho_A}\right)=\left(\frac{1-e^{\frac{-d_A}{\lambda_A \sin\theta}}}{e^{\frac{-(d_A+d_B)}{\lambda_{Si}\sin\theta}}}\right) \qquad \text{(S2)}$$

where d_A is the thickness of the bound F atom and d_B is the thickness of the hydrocarbon layer between the Si crystal and the F atom. The value of SF_A for F 1s photoelectrons is 1.00 and the density of the overlayer was assumed to be the same as for HCC–Si(111) surfaces, 1.9 g cm^{-3}. For F 1s photoelectrons, the value of λ_A is 1.6 nm.[8] Scheme S2 shows the two proposed structures for 4-fluorobenzyl-modified HCC–Si(111) and SiO_x surfaces along with the calculated thickness for d_A and d_B. Since the ratio d_A/d_B is known from Scheme S2, eq S2 can be expressed in terms of d_A and solved using an iterative process. The measured thickness d_A was divided by the calculated thickness of 1 ML of F atoms, 0.13 nm, to give the fractional monolayer coverage of 4-fluorobenzyl groups.

Scheme S2.

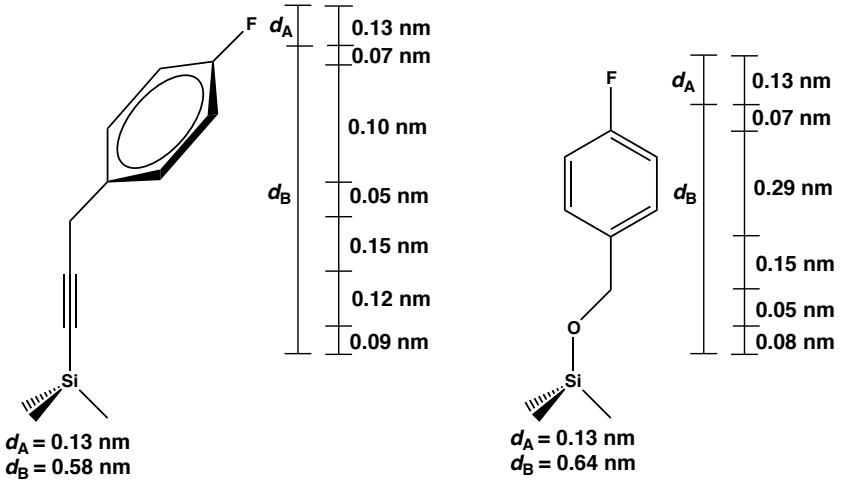

2. Calculation of Surface Recombination Velocity and Surface Trap-State Density. The minority-carrier lifetime (τ) was estimated by fitting the microwave conductivity decay versus time curve to an exponential decay, as described previously.[15-16] The calculated values of τ were converted to surface recombination velocities (S) for wafers of thickness d using[15, 17-18]

$$S = \frac{d}{2\tau} \qquad \text{(S3)}$$

The surface recombination velocity was converted to an effective trap-state density, N_t, using[1, 18]

$$N_t = \frac{S}{\sigma \nu_{th}} \qquad \text{(S4)}$$

where the trap-state capture cross section, σ , was 10^{-15} cm^2 and the thermal velocity of charge carriers, ν_{th}, was 10^7 cm s^{-1}.[18] N_t can be used to estimate the absolute number of electrically active defects per surface Si(111) sites by use of the number density of atop Si sites for an unreconstructed Si(111) surface, $\Gamma_{Si(111)}$, which is 7.83×10^{14} atoms cm^{-2}. Thus, a wafer with surface recombination velocity S has 1 electrically active defect for every $\Gamma_{Si(111)}/N_t$ surface sites.

D. Supporting Figures and Table.

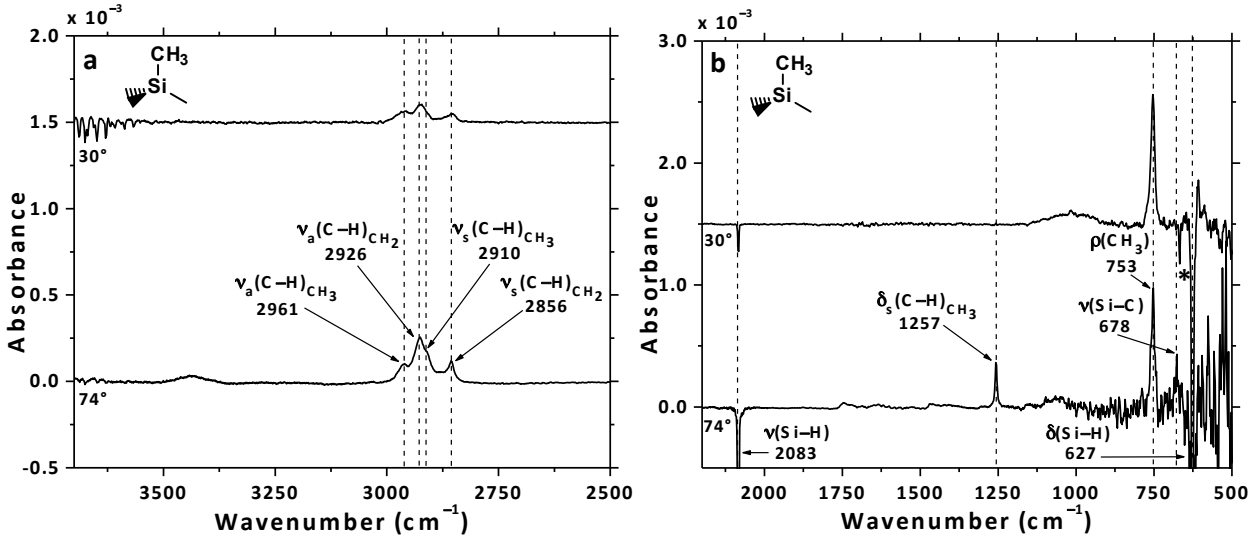

Figure S1. TIRS data for CH_3–Si(111) surfaces, referenced to the H–Si(111) surface, collected at 74° (bottom) and 30° (top) from the surface normal. Panel a shows high-energy region, and panel b shows the low-energy region. The negative peaks in panel b resulted from the H–Si(111) background. A sharp negative peak observed in panel b at 30° incidence marked with ∗ at 667 cm^{-1} resulted from CO_2 in the atmosphere. The subscripts "CH_3" and "CH_2" indicate C–H stretching signals arising from the –CH_3 and –CH_2– groups, respectively. The peak positions and assignments are indicated. The 30° spectrum is offset vertically for clarity.

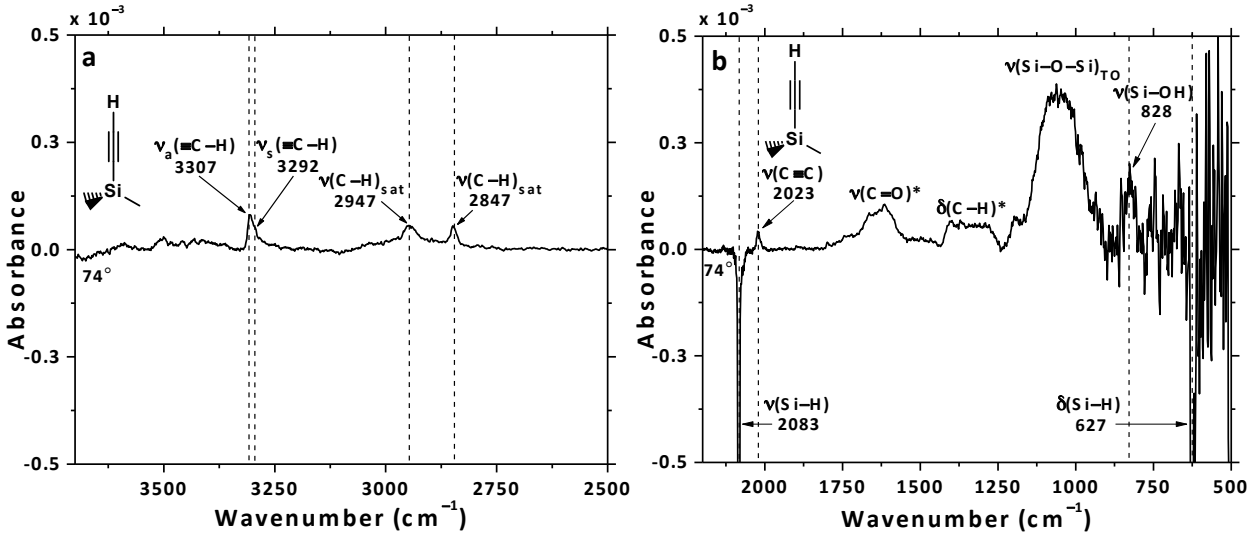

Figure S2. TIRS data for HCC–Si(111) surfaces prepared using DMA, referenced to the H–Si(111) surface and collected at 74° incidence. Panel a shows the high-energy region, and panel b shows the low-energy region. The negative peaks in panel b resulted from the H–Si(111) background. The subscript "sat" is used to denote C–H stretching signals arising from saturated hydrocarbons. The peak positions and assignments (∗ denotes tentative) are indicated in the figure.

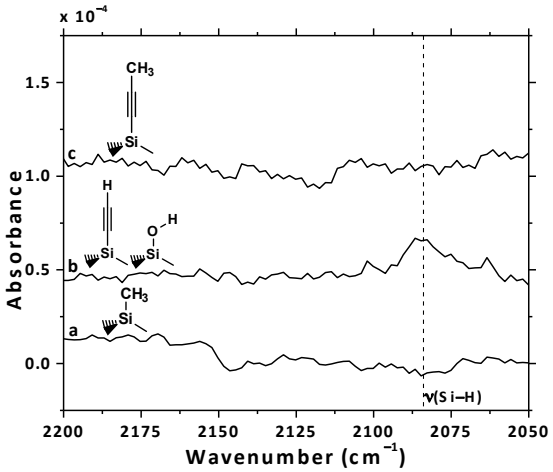

Figure S3. TIRS data for (a) CH_3–Si(111), (b) HCC–Si(111), and (c) CH_3CC–Si(111) surfaces referenced to the SiO_x surface. The position of the Si–H stretching peak is indicated by the dotted line.

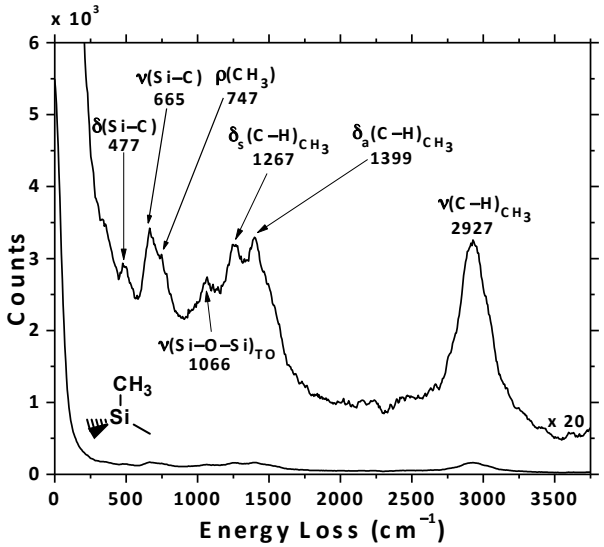

Figure S4. HREELS data for CH_3–Si(111) surfaces. The data were collected in the specular geometry using an incident beam energy of 5.0 eV, and the fwhm of the elastic peak was 13.3 meV. The raw spectrum (bottom) is shown with the magnified spectrum (top) superimposed for clarity. The peak positions and assignments are indicated in the figure.

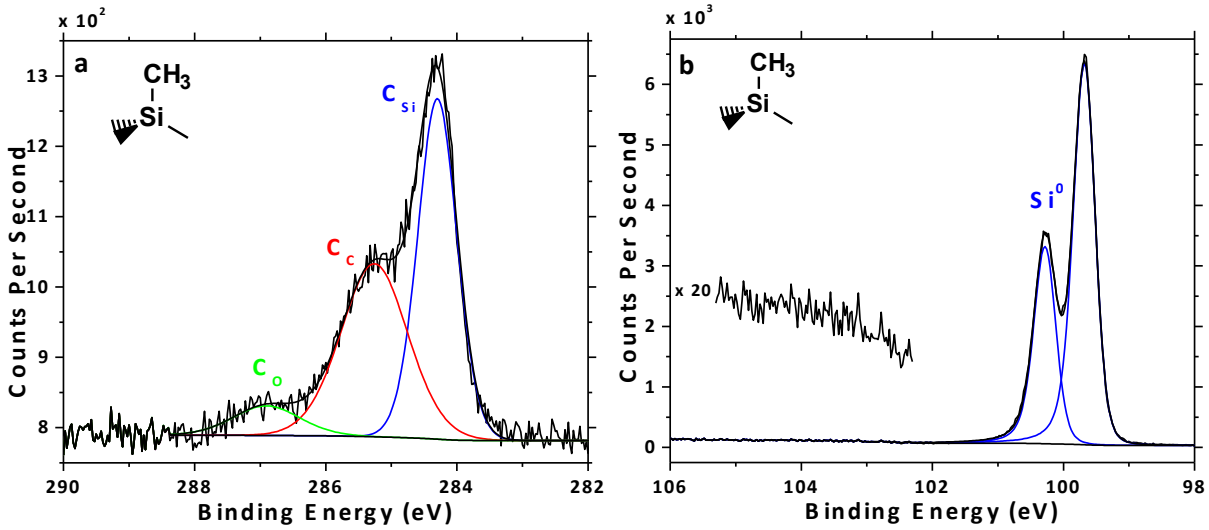

Figure S5. High-resolution XP spectra of the (a) C 1s and (b) Si 2p regions for CH_3–Si(111) surfaces. The low binding-energy C photoemission signal at 284.3 eV has been ascribed to C bound to Si (blue, C_{Si}), with the C 1s signals at 285.2 and 286.4 eV arising from C bound to C (red, C_C) and C bound to O (green, C_O), respectively. The region from 102–105 eV in the Si 2p spectrum is magnified to show the absence of detectable high-order SiO_x.

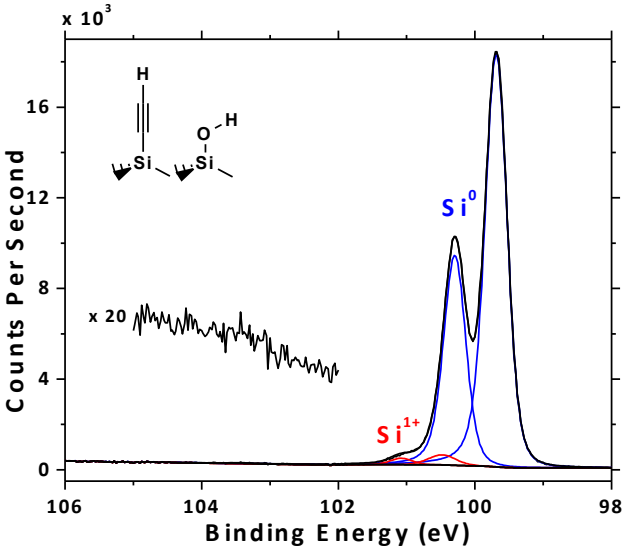

Figure S6. High-resolution XP spectrum of the Si 2p region for HCC–Si(111) surfaces. Contributions from the bulk Si (blue, Si^0) and Si^{1+} (red) species are indicated. The region from 102–105 eV in the Si 2p spectrum is magnified to show the absence of detectable high-order SiO_x.

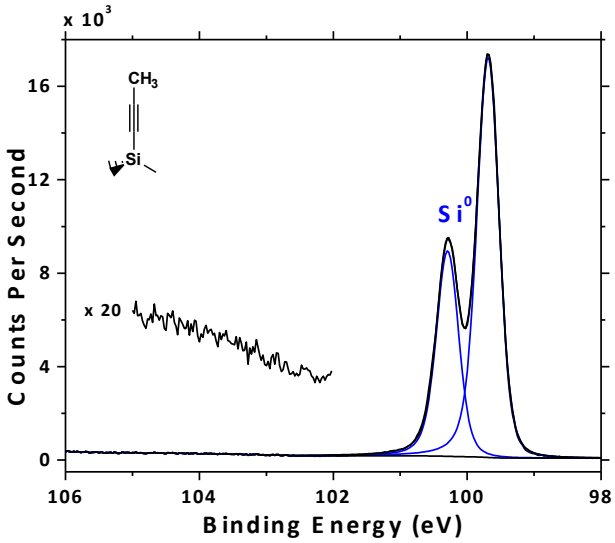

Figure S7. High-resolution XP spectrum of the Si 2p region for CH_3CC–Si(111) surfaces. The Si 2p spectrum showed only a contribution from the bulk Si (blue, Si^0). The region from 102–105 eV in the Si 2p spectrum is magnified to show the absence of detectable high-order SiO_x.

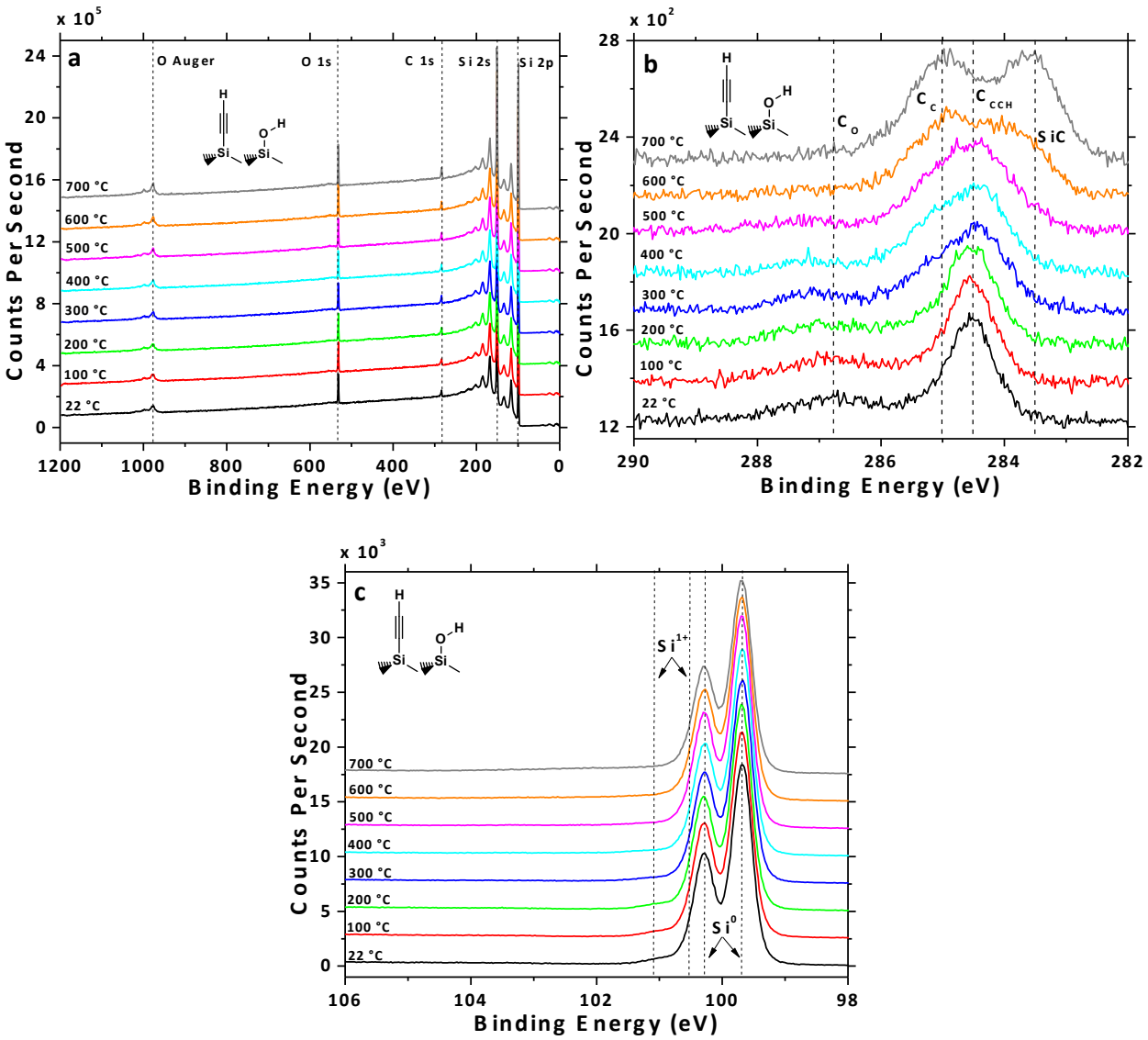

Figure S8. Thermal stability in vacuum of HCC–Si(111) surfaces. The annealing temperature is indicated above each spectrum, and the spectra are offset vertically for clarity. The survey spectra (a) showed the presence of only the Si 2p, Si 2s, C 1s, and O 1s core-level peaks along with the O Auger signal and Si plasmon-loss features. The high-resolution C 1s spectra (b) exhibited the peaks arising from C in the ethynyl group (C_{CCH}) and adventitious C (C_C and C_O). Minimal change in the C 1s spectra was observed upon annealing to 200 °C. Broadening was observed as the C 1s peak at ~285.1 eV (C_C) greatly increased in intensity upon heating to 300–500 °C. Heating to 600–700 °C resulted in the appearance of a new C 1s peak at ~283.5 eV

(SiC). Si 2p spectra (c) showed gradual smoothing of the shoulder indicated as Si^{1+} with increased annealing temperature, indicating the loss of surficial Si–OH and formation of Si–O–Si.

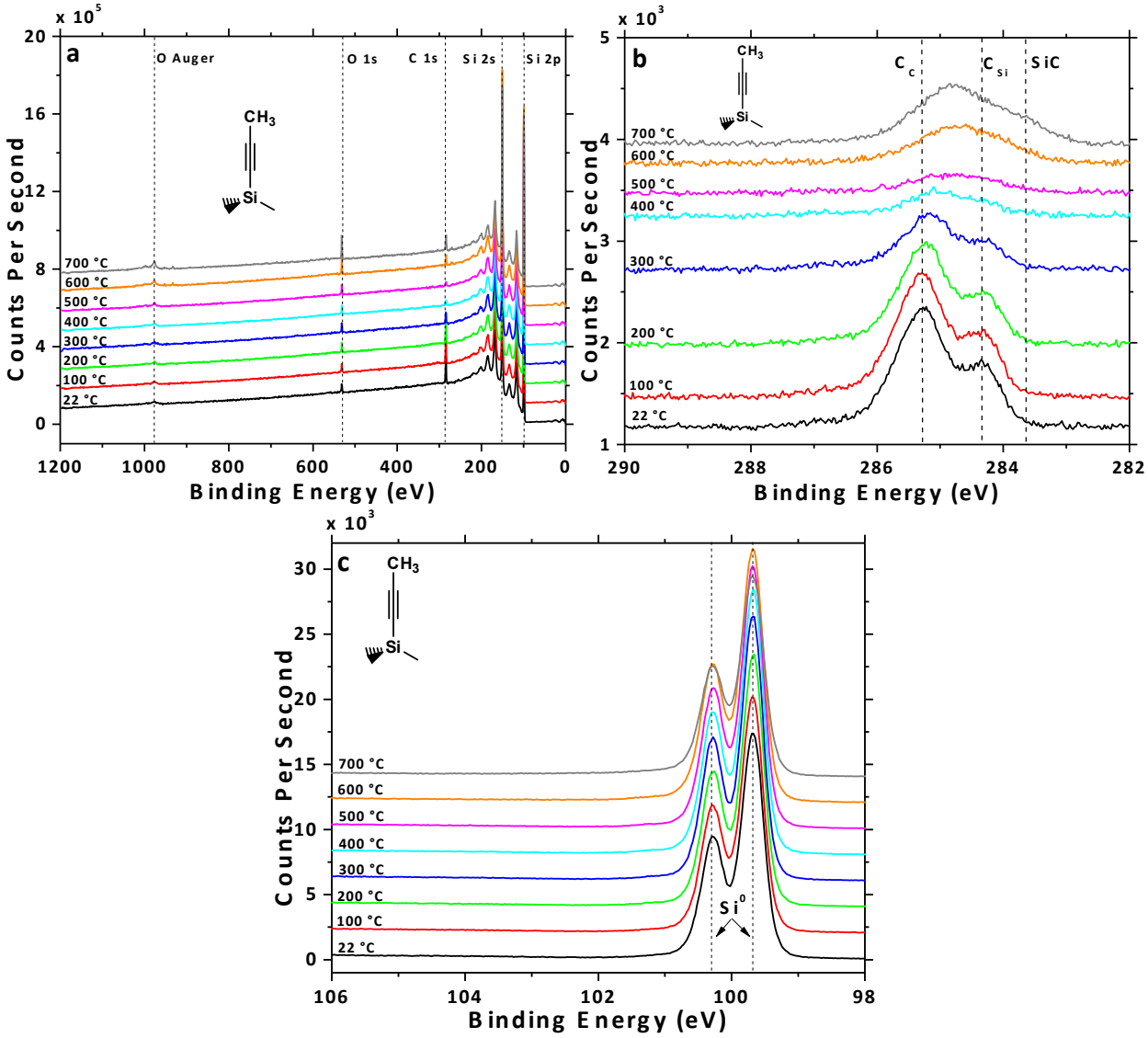

Figure S9. Thermal stability in vacuum of CH_3CC–Si(111) surfaces. The annealing temperature is indicated above each spectrum, and the spectra are offset vertically for clarity. The survey spectra (a) show the presence of only the Si 2p, Si 2s, C 1s, and O 1s core level peaks along with the O Auger signal and Si plasmon-loss features. Annealing to 600 and 700 °C resulted in the observation of a small amount of Cu and Cl, which was likely transferred from the sample holder

to the sample surface during annealing. The high-resolution C 1s spectra (b) showed the behavior of the C bound to Si (C_{Si}) and C bound to C (C_C) peaks with temperature. Upon annealing to 200–500 °C, the overall amount of C decreased. Heating to 600–700 °C resulted in the appearance of a new C 1s peak at ~283.7 eV (SiC). Si 2p spectra (c) showed increased intensity as C was removed from the surface upon annealing to 500 °C, and decreased intensity upon annealing to 600–700 °C.

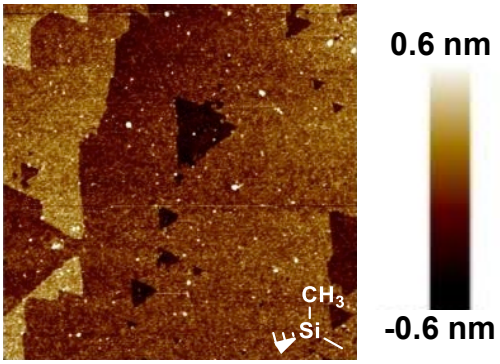

Figure S10. Representative topographical AFM image of the CH_3–Si(111) surface. The image is 1 μm × 1 μm with a z-scale of 1.2 nm (–0.6 to +0.6 nm).

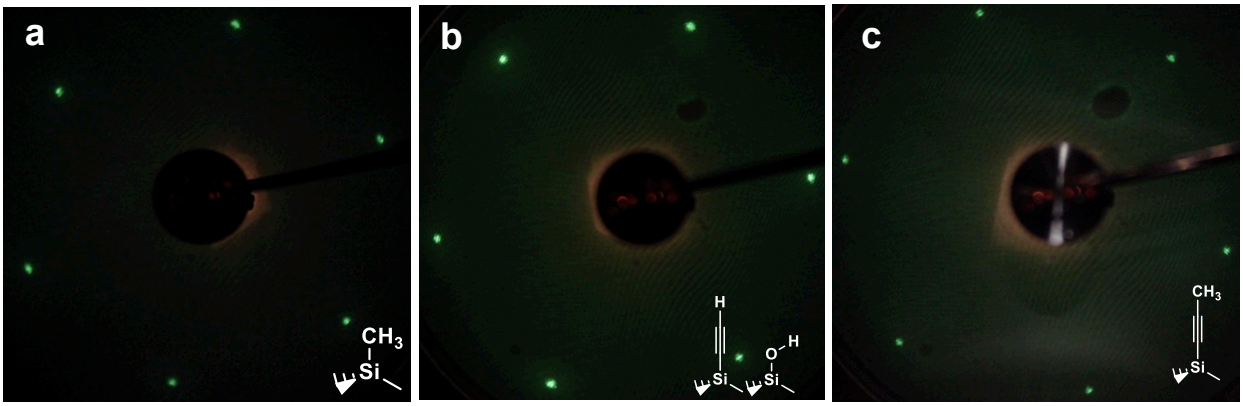

Figure S11. LEED patterns for (a) CH_3–Si(111), (b) HCC–Si(111), and (c) CH_3CC–Si(111) surfaces collected at (a) 43 eV, (b) 40 eV, and (c) 40 eV incident beam energies.

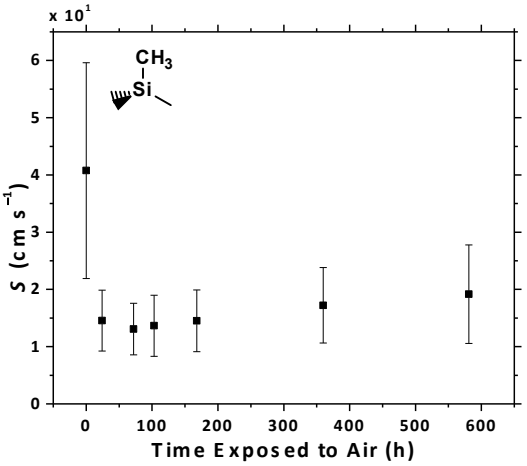

Figure S12. *S* behavior as a function of time exposed to air for CH_3–Si(111) surfaces. The error bars represent 1 standard deviation about the mean.

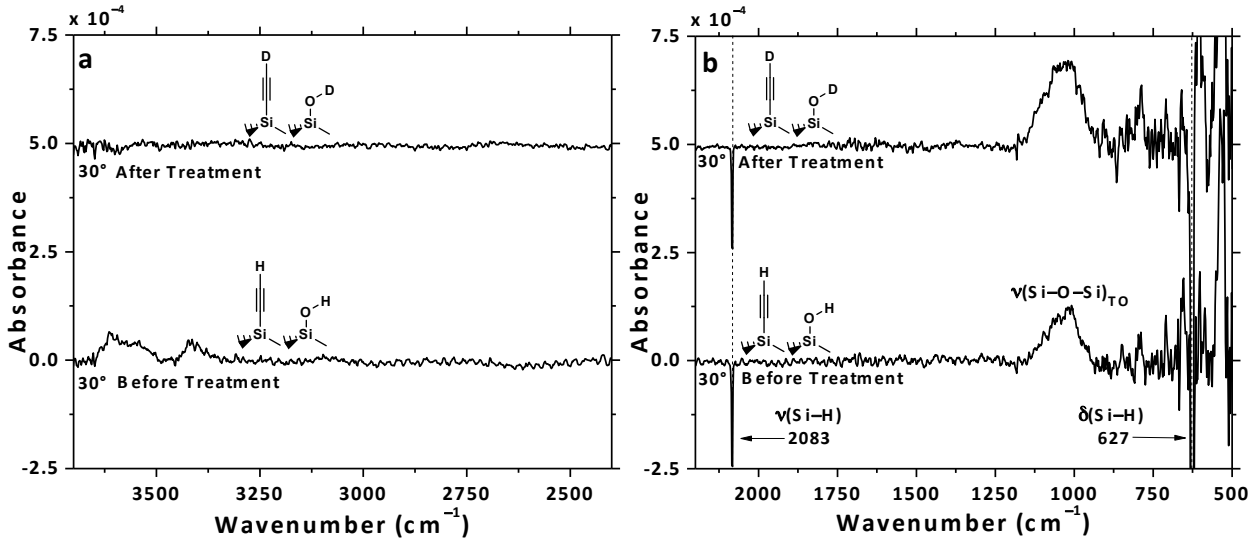

Figure S13. TIRS data for HCC–Si(111) surfaces referenced to the H–Si(111) surface collected at 30° incidence angle before (bottom) and after (top) treatment with *t*-BuLi followed by CD_3OD. Panel (a) shows the high-energy region, and panel (b) shows the low-energy region. The negative peaks in panel (b) resulted from the H–Si(111) background. The absence of any signals attributable to –CCD groups after treatment indicates that the modes observed at 74° are perpendicular to the surface. The spectrum collected after treatment is offset vertically for clarity.

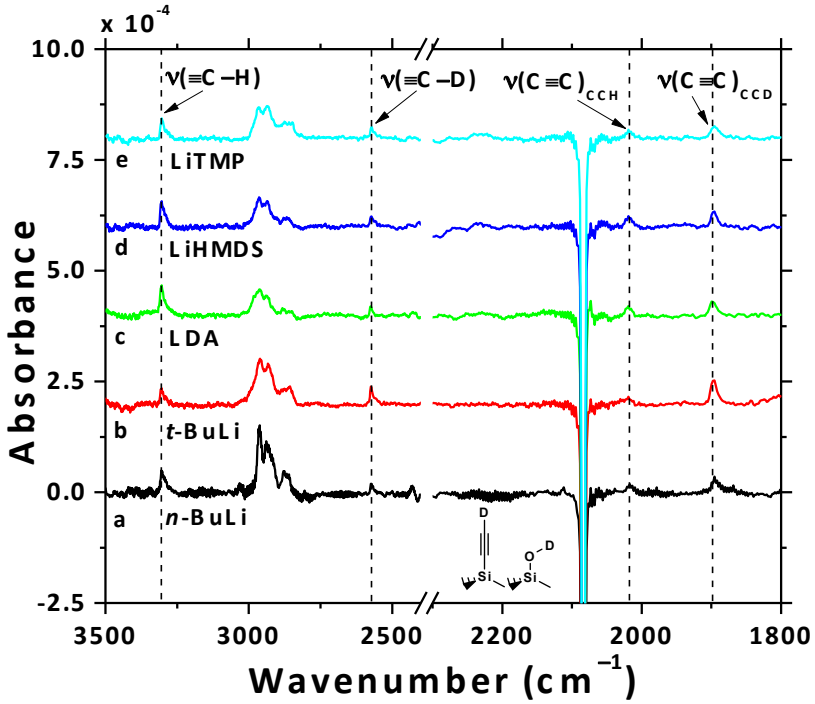

Figure S14. TIRS data collected at 74° incidence angle for HCC–Si(111) surfaces after treatment with (a) *n*-BuLi, (b) *t*-BuLi, (c) LDA, (d), LiHMDS, or (e) LiTMP followed by reaction with CD_3OD. The characteristic peaks corresponding to the –CCH and –CCD surface species are indicated by the dotted lines. The negative peak at 2083 cm^{-1} resulted from the H–Si(111) background. Spectra collected for all bases yielded comparable peaks ascribable to the surface –CCD species. The spectra were offset vertically for clarity.

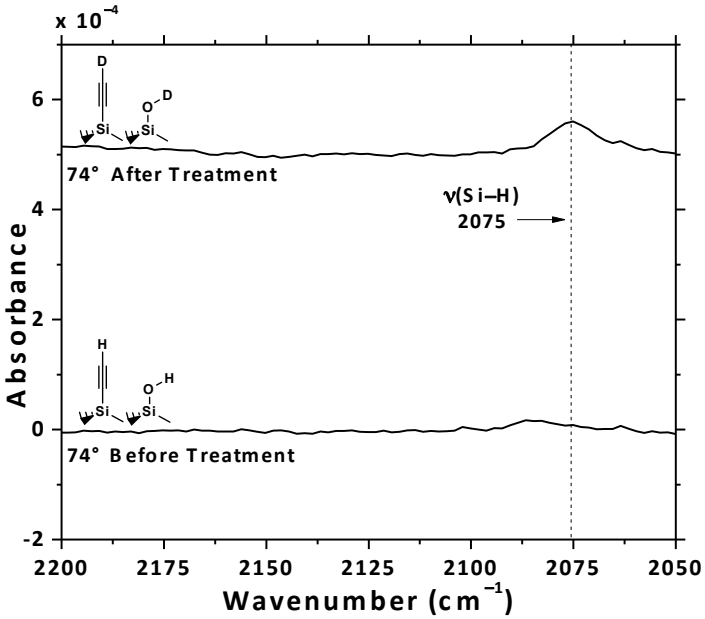

Figure S15. TIRS data collected at 74° incidence angle for HCC–Si(111) surfaces referenced to the SiO_x surface before (bottom) and after (top) treatment with *t*-BuLi followed by CD_3OD. The center of the Si–H stretching peak is indicated by the dotted line, and the broad peak in the top spectrum at 2075 cm^{-1} is ascribed to Si–H stretching.

Table S1. Summary of the positions and assigned modes for the vibrational signatures observed for CH_3–Si(111), HCC–Si(111) DCC–Si(111), and CH_3CC–Si(111) surfaces.

–R	TIRS Frequency (cm^{-1})	HREELS Frequency (cm^{-1})[a]	Assigned Mode[b]	Orientation to Surface[c]
$–CH_3$[23]	2961	2927	$\nu_a(C–H)_{CH_3}$	
	2926	2927	$\nu_a(C–H)_{CH_2}$	
	2910	2927	$\nu_s(C–H)_{CH_3}$	
	2856	2927	$\nu_s(C–H)_{CH_2}$	
	-	1399	$\delta_a(C–H)_{CH_3}$	
	1257	1267	$\delta_s(C–H)_{CH_3}$	⊥
	weak	1066	$\nu(Si–O–Si)_{TO}$	not ⊥
	753	747	$\rho(CH_3)$	not ⊥
	678	665	$\nu(Si–C)$	⊥
	-	477	$\delta(Si–C)$	
–CCH	3620	3625	$\nu(O–H)$	
	3307	3307	$\nu_a(\equiv C–H)$	⊥
	3296	3307	$\nu_s(\equiv C–H)$	⊥
	weak	2954	$\nu(C–H)_{sat}$	
	2019	2032	$\nu(C\equiv C)$	⊥
	1294	1072	$\nu(O–H)$ and $\delta(O–H)*$	⊥
	~1050	1072	$\nu(Si–O–Si)_{TO}$	not ⊥
	920	842	$\delta(O–H)$	⊥
	836	842	$\nu(Si–OH)$	⊥
	-	648	$\nu(Si–C)$	
–CCD	3307	-	$\nu_a(\equiv C–H)$	⊥
	3296	-	$\nu_s(\equiv C–H)$	⊥
	2961	-	$\nu(C–H)_{sat}$	
	2933	-	$\nu(C–H)_{sat}$	
	2856	-	$\nu(O–D)*$	
	2574	-	$\nu_a(\equiv C–D)$	⊥
	2559	-	$\nu_s(\equiv C–D)$	⊥
	2019	-	$\nu(C\equiv C)_{CCH}$	⊥
	1897	-	$\nu(C\equiv C)_{CCD}$	⊥
	~1050	-	$\nu(Si–O–Si)_{TO}$	not ⊥

$-CCCH_3$	2958	3004	$\nu_a(C-H)_{CH_3}$*	not ⊥
	2934	3004	$\nu_f(C-H)_{CH_3}$*	⊥
	2872	3004	$\nu_s(C-H)_{CH_3}$*	⊥
	-	2216	ν(C≡C)	
	-	1435	$\delta_a(C-H)_{CH_3}$	
	1380	1435	$\delta_s(C-H)_{CH_3}$	⊥
	1061	1048	$\nu(Si-O-Si)_{TO}$*	not ⊥
	1033	1048	$\nu(Si-O-Si)_{TO}$* ν(C–C)*	not ⊥
	966	1048	$\rho(CH_3)$*	not ⊥
	-	670	ν(Si–C)	

[a] In some cases, HREELS signals do not resolve multiple vibrational modes that are observed by TIRS. The HREELS signal with the closest energy to the resolved TIRS signal is paired in the table. [b]The symbols ν, δ, and ρ signify stretching, bending, and rocking motions, respectively, with subscripts a, s, and f indicating whether the mode is asymmetric, symmetric, or resulting from Fermi resonance, respectively. Subscripts "CH_3" and "CH_2" indicate C–H stretching signals arising from $-CH_3$ and $-CH_2-$ saturated hydrocarbons, respectively. The subscript "TO" indicates a transverse optical Si–O–Si motion. The subscript "sat" indicates a C–H stretching signal arising from unidentified saturated hydrocarbons. The subscripts "CCH" and "CCD" indicate C≡C stretching peaks arising from –CCH and –CCD groups, respectively. The assignments marked with * are tentative. [c]The orientation of the vibrational mode with respect to the plane of the sample surface determined by TIRS is given.

Supporting Information References

1. O'Leary, L. E.; Rose, M. J.; Ding, T. X.; Johansson, E.; Brunschwig, B. S.; Lewis, N. S. Heck Coupling of Olefins to Mixed Methyl/Thienyl Monolayers on Si(111) Surfaces. *J. Am. Chem. Soc.* **2013**, *135*, 10081-10090.
2. Gleason-Rohrer, D. C.; Brunschwig, B. S.; Lewis, N. S. Measurement of the Band Bending and Surface Dipole at Chemically Functionalized Si(111)/Vacuum Interfaces. *J. Phys. Chem. C* **2013**, *117*, 18031-18042.
3. Rivillon, S.; Chabal, Y. J.; Webb, L. J.; Michalak, D. J.; Lewis, N. S.; Halls, M. D.; Raghavachari, K. Chlorination of Hydrogen-Terminated Silicon (111) Surfaces. *J. Vac. Sci. Technol. A* **2005**, *23*, 1100-1106.
4. Li, Y.; O'Leary, L. E.; Lewis, N. S.; Galli, G. Combined Theoretical and Experimental Study of Band-Edge Control of Si through Surface Functionalization. *J. Phys. Chem. C* **2013**, *117*, 5188-5194.
5. Webb, L. J.; Rivillon, S.; Michalak, D. J.; Chabal, Y. J.; Lewis, N. S. Transmission Infrared Spectroscopy of Methyl- and Ethyl-Terminated Silicon(111) Surfaces. *J. Phys. Chem. B* **2006**, *110*, 7349-7356.
6. Hunger, R.; Fritsche, R.; Jaeckel, B.; Jaegermann, W.; Webb, L. J.; Lewis, N. S. Chemical and Electronic Characterization of Methyl-Terminated Si(111) Surfaces by High-Resolution Synchrotron Photoelectron Spectroscopy. *Phys. Rev. B: Condens. Matter Mater. Phys.* **2005**, *72*, 045317.
7. Briggs, D.; Seah, M. P., *Practical Surface Analysis: Auger and X-Ray Photoelectron Spectroscopy*, 2nd ed.; John Wiley & Sons, Inc.: New York, 1990; Vol. 1.

8. Haber, J. A.; Lewis, N. S. Infrared and X-Ray Photoelectron Spectroscopic Studies of the Reactions of Hydrogen-Terminated Crystalline Si(111) and Si(100) Surfaces with Br_2, I_2, and Ferrocenium in Alcohol Solvents. *J. Phys. Chem. B* **2002**, *106*, 3639-3656.
9. Webb, L. J.; Nemanick, E. J.; Biteen, J. S.; Knapp, D. W.; Michalak, D. J.; Traub, M. C.; Chan, A. S. Y.; Brunschwig, B. S.; Lewis, N. S. High-Resolution X-Ray Photoelectron Spectroscopic Studies of Alkylated Silicon(111) Surfaces. *J. Phys. Chem. B* **2005**, *109*, 3930-3937.
10. van der Marel, C.; Yildirim, M.; Stapert, H. R. Multilayer Approach to the Quantitative Analysis of X-Ray Photoelectron Spectroscopy Results: Applications to Ultrathin SiO_2 on Si and to Self-Assembled Monolayers on Gold. *J. Vac. Sci. Technol. A* **2005**, *23*, 1456-1470.
11. Seah, M. P.; Spencer, S. J. Ultrathin SiO_2 on Si II. Issues in Quantification of the Oxide Thickness. *Surf. Interface Anal.* **2002**, *33*, 640-652.
12. Webb, L. J.; Lewis, N. S. Comparison of the Electrical Properties and Chemical Stability of Crystalline Silicon(111) Surfaces Alkylated Using Grignard Reagents or Olefins with Lewis Acid Catalysts. *J. Phys. Chem. B* **2003**, *107*, 5404-5412.
13. Brown, E. S.; Peczonczyk, S. L.; Maldonado, S. Wet Chemical Functionalization of GaP(111)B through a Williamson Ether-Type Reaction. *J. Phys. Chem. C* **2015**, *119*, 1338-1345.
14. Asami, K.; Hashimoto, K.; Shimodaira, S. XPS Determination of Compositions of Alloy Surfaces and Surface Oxides on Mechanically Polished Iron-Chromium Alloys. *Corros. Sci.* **1977**, *17*, 713-723.

15. O'Leary, L. E.; Johansson, E.; Brunschwig, B. S.; Lewis, N. S. Synthesis and Characterization of Mixed Methyl/Allyl Monolayers on Si(111). *J. Phys. Chem. B* **2010**, *114*, 14298-14302.
16. Lattimer, J. R. C.; Brunschwig, B. S.; Lewis, N. S.; Gray, H. B. Redox Properties of Mixed Methyl/Vinylferrocenyl Monolayers on Si(111) Surfaces. *J. Phys. Chem. C* **2013**, *117*, 27012-27022.
17. Royea, W. J.; Juang, A.; Lewis, N. S. Preparation of Air-Stable, Low Recombination Velocity Si(111) Surfaces through Alkyl Termination. *Appl. Phys. Lett.* **2000**, *77*, 1988-1990.
18. Yablonovitch, E.; Allara, D. L.; Chang, C. C.; Gmitter, T.; Bright, T. B. Unusually Low Surface-Recombination Velocity on Silicon and Germanium Surfaces. *Phys. Rev. Lett.* **1986**, *57*, 249-252.